Energy level structure of $4f5d$ states and the Stokes shift in $LaPO_4:Pr^{3+}$: A theoretical study

A. A. Bagatur'yants,[1] I. M. Iskandarova,[1] A. A. Knizhnik,[1] V. S. Mironov,[1] B. V. Potapkin,[1]
A. M. Srivastava,[2] and T. J. Sommerer[2]
[1]*Kinetic Technologies Ltd., Kurchatov Sq. 1, Moscow 123182, Russia*
[2]*GE Global Research, 1 Research Circle, Niskayuna, New York 12309, USA*
(Received 25 November 2007; revised manuscript received 9 September 2008; published 28 October 2008)

The energy levels and the Stokes shift of the excited $4f^15d^1$ states of Pr^{3+} ions doped into $LaPO_4$ are calculated using a combined theoretical approach. The local structure of the rare-earth site in $LaPO_4$ is obtained from first-principles calculations, while the $4f^15d^1$ states of Pr^{3+} are treated parametrically in terms of a model Hamiltonian. The crystal-field energies of the $5d$ electron of a low-symmetry rare-earth site in $LaPO_4$ are obtained from angular-overlap model calculations. First-principles calculations are performed for $LaPO_4:Ce^{3+}$ used as a reference compound for $LaPO_4:Pr^{3+}$; the geometry parameters of the rare-earth site are determined for the ground state ($4f$) and for the excited ($5d$) state of the central Ce^{3+} ion. It is shown that the $4f$-$5d$ excitation in $LaPO_4:Ce^{3+}$ is accompanied by a strong relaxation of the local structure of the rare-earth site due to rotations of one of the neighboring tetrahedral PO_4 phosphate groups: the coordination number of Ce^{3+} reduces from nine to eight and the average Ce-O distance shortens by about 0.1 Å. This leads to a considerably larger crystal-field splitting energy of the $5d$ states for the excited-state geometry of the cerium site ($\sim$17 700 cm^{-1} vs $\sim$12 000 cm^{-1} in the ground state) and to a large $5d$-$4f$ Stokes shift in $LaPO_4:Ce^{3+}$ (3980 cm^{-1} calculated and 4880 cm^{-1} experimental). The $5d$ crystal-field splitting energies obtained for Ce^{3+} are then employed for calculations of the $4f^15d^1$ energy levels in $LaPO_4:Pr^{3+}$. The calculated Stokes shift in $LaPO_4:Pr^{3+}$ is 3610 cm^{-1}. Due to such a large Stokes shift, in an excited Pr^{3+} ion the lowest $4f^15d^1$ energy level lies below the upper $^1S_0(4f^2)$ level, while in an unexcited ion (in the ground $4f^2$ state) the order of these states is reverse. This fact is responsible for the absence of $4f$-$4f$ emission from the $^1S_0$ state in $LaPO_4:Pr^{3+}$.

DOI: 10.1103/PhysRevB.78.165125 PACS number(s): 71.15.−m, 71.55.−i, 71.70.Ch

I. INTRODUCTION

In recent years there has been an increased interest in the study of vacuum ultraviolet (VUV) spectroscopy of trivalent rare-earth (RE^{3+}) ions due to developments of new luminescent materials for VUV excitations used in plasma display panels, mercury-free lamps, and UV solid-state lasers.[1,2] Intense $4f^N \rightarrow 4f^{N-1}5d$ interconfigurational optical transitions are normally located in the high-energy part of the absorption and emission spectra. These spectra are often difficult to interpret quantitatively due to a complicated energy structure of the excited $4f^{N-1}5d$ states and poorly resolved broad optical bands. Excited $4f^{N-1}5d$ states are usually analyzed using a model based on a parametric Hamiltonian;[3–5] because the number of adjustable parameters is large, these studies have been mainly done for host matrices with a high local symmetry of the rare-earth sites.[6–8] First-principles calculations are of a little use for $4f^{N-1}5d$ states of rare-earth ions due to computational difficulties and an insufficient accuracy. An exception is Ce^{3+} ion having a single electron outside the closed electronic shell, for which first-principles calculations provide more reliable information on the rare-earth sites in the ground $4f$ state and in the excited $5d$ states, including the geometry relaxation effects and Stokes shift.[9–12] These results can be used for the analysis of $4f^{N-1}5d$ states of other rare-earth ions, especially being combined with some empirical regularities in the $4f^N \rightarrow 4f^{N-1}5d$ transition energies of RE^{3+} ions in various host matrices established in the literature. In particular, it has been found that, to a first approximation, the Stokes shift associated with $4f^N \rightarrow 4f^{N-1}5d$ transitions is independent of the type of the lanthanide ion and is mainly determined by the host crystal.[13]

In this paper, we develop a theoretical approach for the analysis of $4f^{N-1}5d$ states that can be applied to low-symmetry rare-earth sites (including C_1 sites, as is the case in $LaPO_4$, see below) and calculations of the Stokes shift. The main idea of this approach is to combine advantages of first-principles calculations in determining the local geometry of Ce^{3+} sites with the efficiency of model calculations for $4f^{N-1}5d$ states of rare-earth ions in host matrices. To avoid a large number of adjustable crystal-field (CF) parameters for $5d$ electrons of RE^{3+} ions in low-symmetry metal sites, we use the angular-overlap model (AOM) to calculate the CF energies of $5d$ states. The computational scheme involves three steps: (a) first-principles calculations are used to determine the local geometry of the Ce^{3+} site in the ground state ($4f$) and in the excited ($5d$) state, (b) the obtained structural data are used to determine the one-electron $5d$ CF energies from AOM calculations, and (c) the $5d$ CF energies are used to calculate the energy level structure of $4f^{N-1}5d$ states and the Stokes shift of the RE^{3+} ions.

This approach is then applied to calculate the $4f^15d^1$ energy level structure and the Stokes shift of Pr^{3+} ions in the $LaPO_4$ host matrix. $LaPO_4:Pr^{3+}$ has attracted considerable interest as a potential quantum splitting phosphor. In Pr^{3+}-doped phosphors, this effect takes place when the lowest $4f^15d^1$ level lies above the $^1S_0(4f^2)$ state (located at about 46 000–48 000 cm^{-1} above the $^3H_4(4f^2)$ ground state). In this case, the $^1S_0$ state is populated due to nonradiative relaxation from the $4f^15d^1$ band; as a result, $4f$-$4f$ transitions

to lower $^{2S+1}L_j(4f^2)$ multiplets of Pr^{3+} can occur, thus producing on average more than one visible photon for every incident ultraviolet photon. Several Pr^{3+}-doped fluorides[14–19] and oxides[20–24] lattices support the radiative transitions from the $^1S_0$ state. In this respect, $LaPO_4:Pr^{3+}$ has an anomalous emission behavior. Despite the fact that in the absorption spectra of $LaPO_4:Pr^{3+}$ the lowest Pr^{3+} $4f^15d^1$ energy level is located above the $^1S_0$ state, the $4f^15d^1 \rightarrow 4f^2$ interconfigurational optical transitions dominate in the emission spectrum of $LaPO_4:Pr^{3+}$; this feature is due to a very large Stokes shift of $4f^15d^1$ states ($\sim$4000 cm^{-1}).[13] In this paper we analyze the origin of the Stokes shift in $LaPO_4:Pr^{3+}$ and we show that it is related to a strong relaxation of the local structure of the rare-earth site upon the $4f \rightarrow 5d$ excitation.

The paper is organized as follows. In Sec. II, we determine the optimized structures of the $LaPO_4:Ce^{3+}$ system in the ground and excited states of Ce^{3+} using a plane-wave pseudopotential density functional theory (DFT) approach. The Stokes shift of $LaPO_4:Ce^{3+}$ is calculated from the differences between the total energies. In Sec. III, we describe AOM calculations for excited $5d$ states of rare-earth ions and calculate the CF energies for Ce^{3+} $5d$ states in $LaPO_4$. The energy spectrum of the $4f^15d^1$ states of $LaPO_4:Pr^{3+}$ is calculated in terms of a parametric model Hamiltonian. In these calculations, we use the $5d$ CF energies (for the ground-state and excited-state geometries) obtained in Sec. II for $LaPO_4:Ce^{3+}$. The Stokes shift of $LaPO_4:Pr^{3+}$ is obtained comparing the calculated $4f^15d^1$ energy spectra for the ground-state and excited-state geometries of the rare-earth site. In Sec. IV, we analyze and discuss our results in light of experimental data for other Pr^{3+}-doped host matrices. The prospects of the use of this approach for calculations of $4f^{N-1}5d$ energy level spectra for other rare-earth ions in low-symmetry sites are also discussed.

II. GEOMETRY OPTIMIZATION OF $LaPO_4:Ce^{3+}$ IN THE GROUND AND EXITED STATES

All geometry optimizations of $LaPO_4$ and $LaPO_4:Ce^{3+}$ are performed using the first-principles DFT approach with a plane-wave (PW) basis set implemented in the PWSCF code.[25] For each chemical element we especially generated ultrasoft pseudopotentials in the Vanderbilt form.[26] Two different pseudopotentials are constructed for the ground and excited states of the Ce^{3+} ion. For the ground state, the $[Kr\ 4d^{10}4f^1]5s^25p^65d^16s^2$ atomic configuration is used, in which the strongly localized $4f$ electron is treated as a core electron; this approach was previously used in the literature for rare-earth sesquioxides and oxysulfides.[27] For the excited state in which the $4f$ electron is excited to a $5d$ orbital, we use the atomic configuration $[Kr\ 4d^{10}]5s^25p^65d^26s^2$. For other elements the configurations are $[Kr\ 4d^{10}]5s^25p^65d^16s^2$ (La), $[Ne]3s^23p^3$ (P), and $[He]2s^22p^4$ (O), respectively.

The PW basis set was expanded up to a cut-off energy of 40 hartree. The k-point sampling is done using a $4\times4\times4$ Monkhorst-Pack grid.[28] All calculations are performed using the gradient-corrected Perdew-Wang exchange-correlation functional.[29] We use temperature smearing of the Fermi surface with $T_{smear}=0.002$ hartree. The geometry optimization process is finished when the largest residual force becomes less than 5×10^{-4} Ry/bohr. It is generally accepted that approximations used in this work provide the geometry of crystal lattices with an accuracy of about 1% (see, for example, Ref. 27), which is quite sufficient for our objectives.

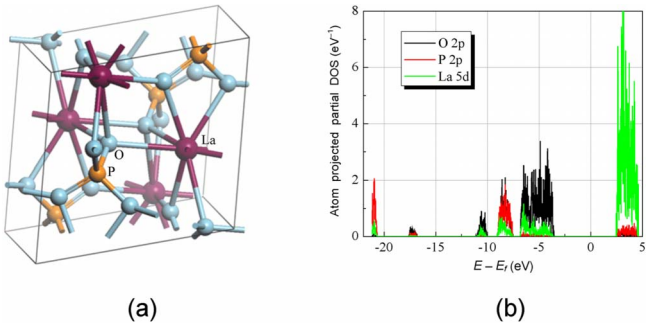

FIG. 1. (Color online) (a) The crystal structure of undoped $LaPO_4$ and (b) its band structure.

First we analyze the electronic structure of undoped $LaPO_4$. This compound crystallizes in a monazite-type structure [a monoclinic system, space group $P2(1)/n$] with the lattice parameters $a=6.8313$ Å, $b=7.0705$ Å, $c=6.5034$ Å, $\alpha=90.00°$, $\beta=103.27°$, $\gamma=90.00°$ (Ref. 30) [Fig. 1(a)]; in this structure, the La site has a very low symmetry (C_1 point group, no symmetry elements).[30–32] The calculated partial density of states (DOS) of the $LaPO_4$ matrix is shown in Fig. 1(b). The conduction band of $LaPO_4$ is mainly represented by the La $5d$ states and the antibonding states of tetrahedral phosphate groups (which are strongly hybridized with the La $5d$ states), while the valence band is mainly formed by O $2p$ states. These results are consistent with the literature data.[33–35] The band gap corresponding to optical measurements is determined by electron excitations from the bonding to antibonding levels of phosphate groups. The calculated band gap ($\sim$6 eV) is smaller than the experimental band gap of 7.8 eV.[35] This is not surprising since the underestimation of the band gap is a general feature of DFT calculations;[36,37] however, it does not influence the geometrical parameters, which are of primary importance in our study.

Then we incorporate the Ce atom into the cell and allow the system to relax in the ground and excited states according to the structure optimization procedure. The extended unit cell of $LaPO_4:Ce^{3+}$ used in calculations contains 24 La atoms, one of which is substituted by the Ce atom. The minimum distance between two doped cerium atoms is 6.5 Å, which is equal to the minimum unit cell parameter.

The average metal-ligand distance for the excited Ce^{3+} ion is found to be $\sim$0.1 Å shorter than in the ground state; in addition, the coordination number of the Ce^{3+} center changes from nine to eight due to rotations of PO_4 groups, which results in the removal of the most distant oxygen atom O7 from the nearest coordination sphere of cerium (Fig. 2).

The Stokes shift ΔS associated with the $4f$-$5d$ electronic transition in $LaPO_4:Ce^{3+}$ is determined by

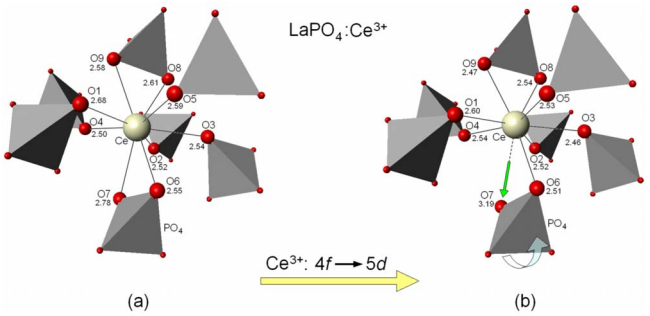

FIG. 2. (Color online) The local structure of the cerium site in $LaPO_4:Ce^{3+}$ obtained from the band DFT calculations, (a) the ground-state geometry, the ground $4f$ state of the central Ce^{3+} ion (large yellow balls), and (b) the excited-state geometry, the excited $5d$ state. In the ground-state geometry, the Ce^{3+} ion is coordinated by nine oxygen atoms (shown as large red balls) from seven phosphate PO_4 groups (shown as gray tetrahedra) with an average Ce-O distance of 2.59 Å. The structure relaxes considerably upon $4f$-$5d$ excitation on Ce^{3+}: due to the rotation of the lower PO_4 group (shown with the curved arrow), the Ce-O7 distance increases by ~0.4 Å, giving rise to the removal of the O7 oxygen atom from the nearest coordination sphere of Ce^{3+}. As a result, the average Ce-O distance shortens by ~0.1 Å (to 2.48 Å) and the coordination number of cerium reduces from nine to eight.

$$\Delta S = (E_1 - E_0) - (E_2 - E_3), \tag{1}$$

where E_0, E_1, E_2, and E_3 are the total energies of the $LaPO_4:Ce^{3+}$ system in the appropriate states, as schematically shown in Fig. 3: E_0 is the energy of $LaPO_4:Ce^{3+}$ in the optimized ground-state geometry (in the ground $4f^15d^0$ configuration of the doped Ce^{3+} ion); E_1 is the energy of $LaPO_4:Ce^{3+}$ system after excitation but before relaxation (the cerium atom in the excited $4f^05d^1$ configuration); E_2 is the energy in the excited $4f^05d^1$ state with the optimized excited-state geometry; E_3 is the energy after the $5d$-$4f$ emission but before relaxation into the ground-state geometry. To calculate these energies, we have performed full geometry optimization of the system for the ground and excited states.

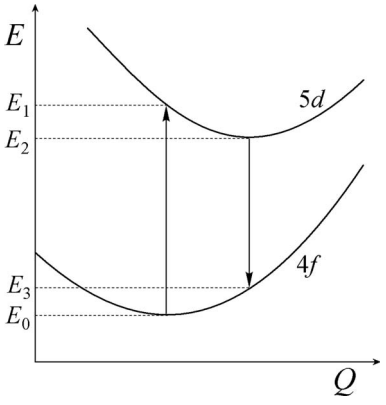

FIG. 3. The origin of the Stokes shift of $4f$-$5d$ electronic transitions in $LaPO_4:Ce^{3+}$. The meaning of the E_0, E_1, E_2, and E_3 energies involved in Eq. (1) in the text is indicated. Here Q is a generalized coordinate along which the system relaxes upon the $4f$-$5d$ transition; it is represented by a combination of local vibrational modes of the rare-earth site. It can be considered as a least-energy path on the potential energy surface of the excited state from the ground-state minimum to the excited-state minimum.

The Stokes shift $\Delta S = 4342\ \text{cm}^{-1}$ obtained from Eq. (1) is in good agreement with the experimental value of 4880 cm^{-1}.[13] Such a large Stokes shift is due to significant changes in the local surrounding of the Ce^{3+} ion upon the $4f$-$5d$ transition; see Fig. 2.

Though DFT calculations provide reasonable results for the Stokes shift in $LaPO_4:Ce^{3+}$, they cannot be directly applied to other $4f^N$ ions with $N>1$ due to the fact that wave functions of $4f^N$ and $4f^{N-1}5d$ states have a complicated multideterminant structure, while DFT calculations use the single-determinant approximation. Below we treat excited $4f^15d^1$ states of Pr^{3+} ions in $LaPO_4$ parametrically in terms of a model Hamiltonian; these calculations are combined with first-principles calculations for the host matrices. Details of this approach are described in the next sections.

III. CALCULATIONS OF THE $4f^15d^1$ ENERGY LEVELS AND THE STOKES SHIFT OF Pr^{3+} ION IN $LaPO_4$

A. Computational model for $4f^{N-1}5d$ states of rare-earth ions

We calculate the energy levels of $4f^{N-1}5d$ states of rare-earth ions in terms of a model Hamiltonian,[3–5]

$$H = H_A + H_{CF}, \tag{2}$$

in which H_A is an "atomic" Hamiltonian involving interactions within the rare-earth ion and H_{CF} is the crystal-field Hamiltonian defined below. H_A can be written as

$$H_A = \Delta E(fd) + H_A(f) + H_A(fd), \tag{3}$$

where $\Delta E(fd)$ is the difference between the centroid energies of the $4f^N$ and $4f^{N-1}5d$ configurations, $H_A(f)$ represents a Hamiltonian for the $4f^{N-1}$ core shell, and $H_A(fd)$ involves interactions between $4f$ and $5d$ electrons. The $H_A(f)$ Hamiltonian is written in a standard parametric form,

$$\begin{aligned} H_A(f) = & \sum_{k=2,4,6} f_k(f)F^k(f) + \alpha L(L+1) \\ & + \beta G(G_2) + \gamma G(R_7) + \sum_i T^i(f)t_i(f) \\ & + \sum_k P^k(f)p_k(f) + \sum_j M^j(f)m_j(f) + \zeta_{4f}\sum_{i=1}^{N-1} \boldsymbol{l}_i\boldsymbol{s}_i, \end{aligned} \tag{4}$$

where $f_k(f)$ and $F^k(f)$ $(k=2,4,6)$ are, respectively, the angular and radial parameters describing the $4f$-$4f$ atomic Coulomb interactions. The $\alpha(f)$, $\beta(f)$, and $\gamma(f)$ parameters refer to two-electron correlation corrections to the Coulomb repulsion, the $T^i(f)$, $P^k(f)$, and $M^j(f)$ operators parametrize the three-electron correlation, electrostatically corrected spin-orbit interaction, and spin-other orbit interaction, respectively.[38–41] The last term in Eq. (4) describes the spin-orbit interaction for $4f$ electrons, where $\boldsymbol{l}_i$ and $\boldsymbol{s}_i$ are, respec-

tively, the operators of the orbital momentum and spin of the ith $4f$ electron in the $4f^{N-1}$ core; in the case of Pr^{3+} ions, $H_A(4f)$ is reduced to the spin-orbit interaction $\zeta_{4f}\boldsymbol{ls}$ only due to the absence of $4f$-$4f$ interactions in the $4f^1$ core shell of the $4f^15d^1$ configuration. The last term $H_A(fd)$ in Eq. (3) is expressed by

$$H_A(fd) = \sum_{k=2,4} f_k(fd)F^k(fd) + \sum_{m=1,3,5} g_m(fd)G^m(fd) + \zeta_{5d}\boldsymbol{ls}, \tag{5}$$

where the radial parameters $F^k(fd)$ and $G^m(fd)$ describe, respectively, the Coulomb and exchange parts of the electrostatic interaction between $4f$ and $5d$ electrons, and $\zeta_{5d}\boldsymbol{ls}$ is the spin-orbit interaction for the $5d$ electron. The crystal-field Hamiltonian H_{CF} for the $4f^{N-1}5d$ configuration is written as

$$H_{CF} = H_{CF}(f) + H_{CF}(d) + H_{CF}(fd), \tag{6}$$

where $H_{CF}(f)$ and $H_{CF}(d)$ describe the anisotropic part of ion-lattice interactions for $4f$ and $5d$ electrons, respectively. They are expressed as

$$H_{CF}(f) = \sum_{kq} B_q^k(f)C_q^{(k)}(f), \tag{7}$$

$$H_{CF}(d) = \sum_{kq} B_q^k(d)C_q^{(k)}(d), \tag{8}$$

where $B_q^k(f)$ and $B_q^k(d)$ are the crystal-field parameters and $C_q^{(k)}(f)$ and $C_q^{(k)}(d)$ are spherical tensor operators for the $4f^{N-1}$ core and for the $5d$ electron, respectively; here $k=2,4,6$ for $4f$ electrons and $k=2,4$ for the $5d$ electron, and q runs from $-k$ to k (Ref. 41) (see also Refs. 3–5 and Refs. 38–40). The $H_{CF}(fd)$ term in Eq. (6) is the odd-parity crystal-field interaction that mixes the $4f^N$ and $4f^{N-1}5d$ configurations

$$H_{CF}(fd) = \sum_{kq} B_q^k(fd)C_q^{(k)}(fd), \tag{9}$$

where $k=1$, 3, and 5.

In this paper, we focus on the analysis of $4f^15d^1$ energy levels and the $5d$ Stokes shift of Pr^{3+} ions in $LaPO_4$. Though calculations for Pr^{3+} ions are simpler than for other many-electron rare-earth ions due to considerable simplifications in the $H_A(f)$ Hamiltonian (4), in the case of $LaPO_4:Pr^{3+}$ the model Hamiltonian (1) still involves several tens of adjustable CF parameters $B_q^k(f)$, $B_q^k(d)$, and $B_q^k(fd)$ due to a low symmetry of the rare-earth site. This problem is even more serious for the excited-state geometry of the rare-earth site in $LaPO_4$. We need, therefore, to simplify the model to reduce the number of parameters without a significant loss of accuracy. For this purpose, we neglect less important interactions and use some approximations:

(a) In the absence of the strongest $4f$-$4f$ interactions $H_A(f)$ in the $4f^{N-1}$ core for the excited $4f^15d^1$ states of Pr^{3+}, the next strong interactions are the Coulomb interaction $H_A(fd)$ between $4f$ and $5d$ electrons and the crystal-field splitting $H_{CF}(d)$ for the $5d$ electron. In fact, the $H_A(fd)$ and $H_{CF}(d)$ interactions are comparable in magnitude ($\sim$10 000–15 000 cm^{-1}), so they are both taken into account.

(b) The CF splitting of $4f$ electrons $H_{CF}(f)$ is neglected in calculations of $4f^15d^1$ energy levels. This approach is based on two arguments. First, the $4f$ CF splitting energy $H_{CF}(f)$ of rare-earth ions in host matrices is generally much smaller than the leading interactions $H_A(fd)$ [Eq. (5)] and $H_{CF}(d)$ [Eq. (8)] (on the order of 10 000 cm^{-1}): the $4f$ CF splitting is normally few hundreds of cm^{-1} (very seldom it can reach 1000 cm^{-1}) (Ref. 42); in $LaPO_4$ and other rare-earth host matrices with a monazite-type structure it is about 500 cm^{-1}.[43] Therefore, errors in the determining energy positions of $4f^{N-1}5d^1$ states resulting from neglecting the $H_{CF}(4f)$ term in Eq. (2) are also of order few hundreds of cm^{-1}, which is considerably smaller than the $5d$ Stokes shift in $LaPO_4$ ($\sim$4000–5000 cm^{-1}).[13] In fact, this is smaller than or comparable to the uncertainty in calculations of the energy positions of excited $5d$ levels and the experimental accuracy in the determining the Stokes shift of rare-earth ions. Therefore, omitting the $H_{CF}(f)$ term in Eq. (3) is rather safe. Second, this approximation eliminates the problem of a large number of CF parameters for $4f$ electrons. For the C_1 point symmetry of the rare-earth site in $LaPO_4$, there are as many as 27 $B_q^k(f)$ CF parameters involved in the CF Hamiltonian $H_{CF}(f)$ [Eq. (7)]; their determining by fitting to experimental data is difficult and rather unreliable.[44–46]

(c) The CF splitting for the $5d$ electron is treated in terms of the angular-overlap model. Details of this approach are discussed below.

(d) The odd-parity CF Hamiltonian $H_{CF}(fd)$ [Eq. (9)] is neglected. Though taking $H_{CF}(fd)$ into account is important in intensity calculations, it has a small influence on the energy positions of $4f^15d^1$ states.[2–8]

These points reflect a compromise between the complexity and accuracy of calculations for $4f^{N-1}5d$ states of rare-earth ions in low-symmetry host matrices. The main attention is paid to the strongest ion-lattice interaction for $5d$ electrons, while taking into account all f-f and f-d atomic interactions, which are also strong. All calculations are performed using a suite of specially designed routines.

B. Calculations of crystal-field energies of 5*d* states of rare-earth ions in $LaPO_4$: angular-overlap model

The major problem in calculations of the $4f^15d^1$ energy levels of $LaPO_4:Pr^{3+}$ concerns an adequate description of the $5d$ CF splitting pattern for low-symmetry rare-earth sites. With $k=2$, 4 and $|q| \le k$, there are 14 $B_q^k(d)$ parameters in the CF Hamiltonian $H_{CF}(d)$ [Eq. (8)]. For metal sites with higher symmetry the number of independent CF parameters may be considerably smaller. Therefore, the use of the standard CF parametrization (8) is efficient only for rare-earth sites of higher symmetry, when the number of adjustable $B_q^k(d)$ parameters is not too large. Some examples of such CF calculations for excited $4f^{N-1}5d$ states of rare-earth ions have been described in the literature.[2–8,47–49] In this respect, the case of $LaPO_4$ is extremely unfavorable for these CF calculations

due to the presence of the maximal number of parameters: in fact, 14 $B_q^k(d)$ parameters cannot be fitted in a reliable way to a very limited number of resolved $5d$ levels in the experimental $4f$-$5d$ absorption and excitation spectra. On the other hand, in order to calculate the $5d$ Stokes shift in $LaPO_4:Pr^{3+}$ or $LaPO_4:Ce^{3+}$ we need to determine the $5d$ CF energies not only for the ground-state ($4f$) geometry of the rare-earth site, but for the excited-state ($5d$, relaxed) geometry too. Obviously, this cannot be done in terms of the $B_q^k(d)$ parametrization (8) due to the absence of the experimental data on the high-lying $5d$ levels of rare-earth ions in the $5d$-$4f$ emission spectra (since the $5d$-$4f$ transitions occur normally from the lowest $4f^{N-1}5d$ level only).

In this paper, we use an alternative approach for CF calculations of $5d$ states of rare-earth ions in terms of the AOM (Refs. 50–54), which is outlined below. The angular-overlap model is based on the idea that the CF potential for d electrons can be represented by a superposition of separate contributions $v(k)$ from individual metal-ligand pairs k involved in the nearest coordination sphere of the metal ion,

$$H_{\mathrm{CF}}(d) = \sum_k v(k), \tag{10}$$

where each contribution $v(k)$ is assumed to be axially symmetric with respect to the corresponding metal-ligand axis. In the local coordinate frame associated with the given pair k with the quantization axis being parallel to the metal-ligand axis, the one-electron operator $v(k)$ is diagonal in the $|lm\rangle$ basis set of d_m orbitals, i.e., $\langle m|v(k)|m'\rangle = e^k_{|m|}d_{mm'}$, where m is the projection of the orbital momentum of d electrons. The quantities $e^k_{|m|}$ are the destabilization energies of d_m orbitals resulting from the local metal-ligand interaction k. Since the destabilization energies of d_0 and $d_{\pm 1}$ orbitals originate from the overlap of metal and ligand orbitals of the σ and π type, respectively, they are denoted as $\langle 0|v(k)|0\rangle = e_\sigma$ and $\langle \pm 1|v(k)|\pm 1\rangle = e_\pi$; the diagonal matrix element for $d_{\pm 2}$ orbitals can be set to zero ($e^k_{|m=\pm 2|}=0$) without loss of generality (especially when ligands have no filled d orbitals). In the common coordinate frame matrix elements of the operator $v(k)$ are related to the $e^k_{|m|}$ quantities according to the transformational properties of the central metal orbitals d_m under rotation,

$$\langle m|v(k)|m'\rangle = \sum_{\mu=-2}^{2} D^2_{\mu m}(\theta_k,\varphi_k)^* D^2_{\mu m'}(\theta_k,\varphi_k) e^k_{|\mu|}, \tag{11}$$

where $D^2_{\mu m}(\theta_k,\varphi_k)$ are the Wigner second-rank rotation functions with θ_k and φ_k being the angular coordinates of the kth ligand. Then according to Eq. (10), the matrix elements of the global CF Hamiltonian $H_{\mathrm{CF}}(d)$ are finally written as

$$\langle m|H_{\mathrm{CF}}(d)|m'\rangle = \sum_k \sum_{\mu=-2}^{2} D^2_{\mu m}(\theta_k,\varphi_k)^* D^2_{\mu m'}(\theta_k,\varphi_k) e^k_{|\mu|}. \tag{12}$$

The contribution to $H_{\mathrm{CF}}(d)$ from the kth metal-ligand pair is parametrized by two AOM parameters e^k_σ and e^k_π; therefore, in general case there is a total of $2n$ parameters for n ligands involved in the nearest coordination sphere of the metal atom. However, for metal sites with the same type of monoatomic ligands (such as O, F, or Cl) the number of independent parameters can be considerably reduced by using an analytical approximation for the radial dependence for the AOM parameters, $e_{\sigma,\pi}(R) = e_{\sigma,\pi}(R_0)(R/R_0)^n$, where R_0 is the average metal-ligand distance. In this way, the $H_{\mathrm{CF}}(d)$ Hamiltonian can be parametrized by only two adjustable parameters $e_\sigma(R_0)$ and $e_\pi(R_0)$, regardless of the specific geometry of the metal site. An important advantage of this CF parametrization is that the AOM parameters are transferable between different host matrices with the same types of ligands [in contrast to the $B_q^k(d)$ parameters in Eq. (8), which are not transferable]. In other words, if the $e_\sigma(R_0)$ and $e_\pi(R_0)$ parameters are once determined for a certain host matrix, they can be used [with a distance correction $e_{\sigma,\pi}(R) = e_{\sigma,\pi}(R_0)(R/R_0)^n$] for other host matrices with the same type of ligands. This enables to predict the CF energies of d states of a given metal ion in host matrices with unknown spectroscopic characteristics. In many cases AOM calculations can be further simplified by fixing the e_σ/e_π ratio, which can be estimated from the experimental data or theoretically using the fact that AOM parameters are approximately proportional to the square overlap integrals between metal and ligand orbitals of σ and π types, $e_\sigma \sim S^2_{s\sigma} + S^2_{p\sigma}$ and $e_\pi \sim S^2_{p\pi}$.[55–59] With these approximations, $H_{\mathrm{CF}}(d)$ is parametrized by the only adjustable parameter e_σ, which can easily be determined from spectroscopic data for d electrons. This has an advantage that the only experimental d-d transition energy is needed to determine e_σ, such as the total CF splitting energy of $5d$ states; this value is well documented for rare-earth ions in many host lattices.[13] Therefore, this approach can provide a very compact and efficient description of the CF splitting patterns of d electrons, irrespective of the specific local structure of the metal site.

AOM has been widely used in the literature for the analysis of optical and magnetic properties of $3d$ transition-metal compounds.[50–62] The application of AOM calculations to excited $5d$ states of rare-earth ions is based on the fact that characteristics of $3d$ electrons of transition-metal ions and $5d$ electrons in the excited $4f^{N-1}5d$ states of rare-earth ions are similar (such as the radial extension and CF energies). Below we apply this approach to analyze the CF splitting pattern of $5d$ states of Ce^{3+} ions in $LaPO_4$ and then we use these results for $4f^15d^1$ energy level calculations in $LaPO_4:Pr^{3+}$.

C. Calculations of the $5d$ CF energies and the Stokes shift in $LaPO_4:Ce^{3+}$

First, we determine the AOM parameters for $LaPO_4:Ce^{3+}$ using the ground-state geometry of the cerium site in Ce^{3+} ion obtained from band DFT calculations [see Sec. II, Fig. 2(a)]. Only the nearest oxygen atoms (with $R_{\text{Ce-O}} < 3$ Å) are taken into account. The distance dependence of the e_σ and e_π parameters is approximated by the equation $e_{\sigma,\pi}(R) = e_{\sigma,\pi}(R_0)(R/R_0)^n$, where $R_0 = 2.59$ Å is the average Ce-O distance in the Ce site. The value of the power index n was discussed in the literature.[55–59,62,63] For d electrons the electrostatic point-charge CF model gives $n=5$; however, the actual value of n is often substantially different

TABLE I. Calculated and experimental crystal-field splitting patterns of the $5d$ electron of Ce^{3+} ion in $LaPO_4$.

One-electron crystal-field energies of $5d$ states (cm^{-1})		
Ground-state geometry ($4f$)		Excited-state geometry ($5d$)
Expt.[a]	Calc.	Calc.
0	0	0
2430	1592	6678
5210	5237	10814
10100	9858	13427
11910	12018	17673

[a]References 70 and 71.

ranging from ~3.0 to ~7.5. First-principles calculations for various transition-metal ($3d$) compounds also predict some deviations from $n=5$.[58,64] In most cases, n fluctuates around 5; smaller n is preferentially observed in metal sites with short metal-ligand distances and small coordination numbers, while $n>5$ is more typical of longer metal-ligand distances and larger coordination numbers. The n value for $5d$ electrons can be estimated from the pressure dependence of $4f$-$5d$ optical transitions.[65,66] However, direct information on the index n for excited $5d$ states of rare-earth ions has been recently obtained from relativistic first-principles calculations.[67–69] It has been found from the analysis of the radial dependence of the calculated $10Dq$ CF energy of excited $5d$ states of RE^{3+} ions in cubic metal sites (CaF_2, SrF_2, and BaF_2 fluorite matrices)[68] and in octahedral sites (Cs_2NaYCl_6 elpasolite)[69] that in all cases $n>5$. In the $LaPO_4$ host matrix with large La-O distances and oxygen ligands, n is expected to be somewhat larger than in fluorides and chlorides; thus we use $n=7$. In particular, such a value was obtained from the experimental pressure dependence of the $10Dq$ CF energy in the $Mn^{II}Cl_6^{4-}$ complex, in which the metal-ligand distance is close to that in $LaPO_4$ (~2.5 Å).[63]

The AOM parameters can be determined by fitting the calculated $5d$ energy levels [obtained by diagonalization of the $H_{CF}(d)+\zeta_{5d}\boldsymbol{ls}$ Hamiltonian, in which the experimental spin-orbit coupling constant for $5d$ electron of Ce^{3+} is used, $\zeta_{5d}=1082$ cm^{-1}][5] to the experimental energy positions of the $5d$ states in $LaPO_4:Ce^{3+}$, which are known from the resolved $4f$-$5d$ absorption spectra: 36 630 cm^{-1} (273 nm), 39 060 cm^{-1} (256 nm), 41 840 cm^{-1} (239 nm), 46 730 cm^{-1} (214 nm), and 48 540 cm^{-1} (206 nm).[70,71] In $LaPO_4:Ce^{3+}$ simultaneous fitting of e_σ and e_π leads to a rather uncertain e_π/e_σ ratio due to a very flat minimum in the least-squares sum. However, this feature is specific to $LaPO_4:Ce^{3+}$ only, because similar AOM calculations for Ce^{3+} ion in other oxide and fluoride host matrices give normally a distinct minimum with a stable e_π/e_σ ratio around 0.2–0.25; a similar ratio was also obtained from AOM calculation in many $3d$ compounds.[55–59] Thus for $LaPO_4:Ce^{3+}$ we use $e_\pi/e_\sigma=0.25$; in this approach, $e_\sigma(R_0)$ is the only parameter to be determined. The total CF energy of $5d$ states $\Delta E_{CF}(5d)=11\,910$ cm^{-1} is reproduced at $e_\sigma(R_0)=7500$ cm^{-1} with good agreement between the calculated and experimental CF energy levels (Table I).

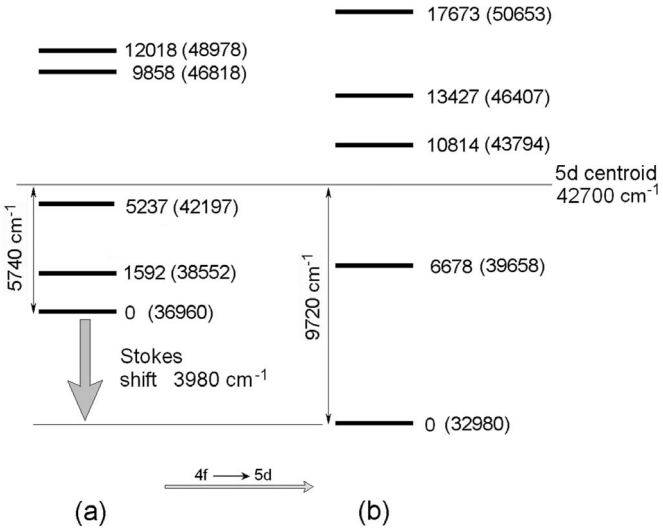

FIG. 4. The origin of the Stokes shift in $LaPO_4:Ce^{3+}$, (a) CF splitting of $5d$ states of Ce^{3+} in the ground-state geometry (in the $4f$ state), (b) CF splitting of $5d$ states of Ce^{3+} in the excited-state geometry (in the excited $5d$ state). The absolute energy positions of $5d$ levels are indicated in parentheses.

With the obtained AOM parameters [$e_\sigma(R_0)=7500$ cm^{-1} and $e_\pi(R_0)/e_\sigma(R_0)=0.25$] we can calculate the $5d$ CF splitting pattern for the excited-state geometry of the Ce site in $LaPO_4$ using the radial dependence $e_{\sigma,\pi}(R)=e_{\sigma,\pi}(R_0)(R/R_0)^n$. Due to a substantial relaxation of the local structure [involving the removal of one of the oxygen atoms from the nearest coordination sphere of Ce^{3+} ion and the reduction by ~0.1 Å in the average Ce-O distance; see Fig. 2(b)], the $5d$ CF energy increases from ~12 000 to ~17 700 cm^{-1} and the CF splitting pattern changes considerably (Table I). These data can be employed to calculate the Stokes shift associated with $5d$ states. We suppose that the Stokes shift is mainly due to the increase in the $5d$ CF splitting energy in the excited-state geometry, whereas the shift of the $5d$ centroid energy (measured from the ground $4f$ state) is less important. In fact, the latter suggestion is involved in the basic Hamiltonian (3), in which the difference $\Delta E(fd)$ between the $4f$ and $5d$ centroids is constant. This is also consistent with the results of first-principles calculations for $4f$-$5d$ transitions of rare-earth ions in various host matrices which show that the energy positions of the $5d$ centroid is rather insensitive to the host matrix.[66]

In this approach, the $5d$ Stokes shift of $LaPO_4:Ce^{3+}$ can be calculated according to the scheme shown in Fig. 4. First, the relative $5d$ centroid energies (measured from the lowest $5d$ level) are calculated for the $5d$ CF splitting patterns for the ground-state and excited-state geometries of the cerium site, and then these two centroids are set to the absolute $5d$ centroid energy obtained from the experimental $4f$-$5d$ absorption spectra (42 700 cm^{-1}; see Fig. 4). The $5d$ Stokes shift is determined by the difference of the energy distances between the $5d$ centroid position and the energy of the lowest $5d$ level calculated in the excited-state and ground-state geometries. In this way, we obtain 3980 cm^{-1} for the Stokes shift in $LaPO_4:Ce^{3+}$; see Fig. 4. This value is consistent with that obtained above from the first-principles calculations

(4342 cm^{-1}; see Sec. II) and reasonably agrees with the experimental Stokes shift of $LaPO_4:Ce^{3+}$, 4880 cm^{-1}.[13]

D. $4f^15d^1$ energy levels and the Stokes shift of Pr^{3+} ions in $LaPO_4$

Using the model described in Sec. III A and the AOM parameters obtained for $LaPO_4:Ce^{3+}$ we can calculate the $4f^15d^1$ energy levels and the Stokes shift in $LaPO_4:Pr^{3+}$. Since electrostatic interactions are absent in the $4f^{N-1}$ core of the $4f^15d^1$ excited states of Pr^{3+}, only fd atomic parameters involved in the $H_A(fd)$ Hamiltonian (5) are needed for calculations. Several sets of these parameters were reported in the literature.[5,6,8] Since the $F^k(fd)$ and $G^m(fd)$ parameters obtained from the standard atomic calculations[72] are rather overestimated, in our calculations for $LaPO_4:Pr^{3+}$ we use the experimental parameters $F^2(fd)=21\,941$, $F^4(fd)=16\,690$, $G^1(fd)=10\,374$, $G^3(fd)=12\,369$, $G^5(fd)=8786$, $\zeta_{4f}=926$, and $\zeta_{5d}=1014$ cm^{-1} obtained by fitting to the experimental $4f^15d^1$ energy levels of free (gaseous) Pr^{3+} ions.[8]

We assume that the Ce^{3+} and Pr^{3+} sites in $LaPO_4$ are close to each other in the geometry parameters and characteristics of $5d$ orbitals, so the same AOM parameters are used for Ce and Pr. It is noteworthy that in our calculations the representation of the $5d$ CF Hamiltonian differs from the standard form (8) written in terms of the $B_q^k(d)$ parameters and the $C_q^{(k)}(d)$ spherical tensor operators: $H_{CF}(d)$ is specified by the set of one-electron matrix elements $\langle m|H_{CF}(d)|m'\rangle$ (MEs) obtained from Eq. (12). In fact, these two representations of the $5d$ CF Hamiltonian are equivalent since there is a one-to-one correspondence between the sets of $\langle m|H_{CF}(d)|m'\rangle$ MEs and $B_q^k(d)$ parameters. For practical calculations it is more convenient to transform MEs from the $|lm\rangle$ basis set of d_m orbitals to real (Cartesian) d_α orbitals, $\langle\alpha|H_{CF}(d)|\beta\rangle$ (where α and β run over the x^2-y^2, xy, z^2, zx, and yz indices of real $5d$ orbitals). The calculated $\langle\alpha|H_{CF}(d)|\beta\rangle$ MEs for ground-state and excited-state geometries for the rare-earth site in $LaPO_4$ are listed in Table II. Note that no symmetry elements or approximate symmetry are assumed for the metal site in these CF calculations.

The $4f^15d^1$ energy levels of $LaPO_4:Pr^{3+}$ are obtained for the ground-state and excited-state geometries of the praseodymium site from the diagonalization of Hamiltonian (2) in the full basis set of $4f^15d^1$ wave functions (involving a total of 140 two-electron states); their energy positions and the compositions of the wave functions calculated for the ground-state geometry are presented in Table III. For the ground-state geometry, the absolute energy position of the lowest $4f^15d^1$ state with respect to the $4f^2$ ground state is determined from the empirical regularity that the energy difference between the lowest $4f^15d^1$ level of Pr^{3+} and the lowest $5d$ level of Ce^{3+} in the host matrix is a constant value of $12\,240\pm750$ cm^{-1}.[13] The experimental energy of the lowest $4f$-$5d$ transition in $LaPO_4:Ce^{3+}$ is 36 630 cm^{-1} (273 nm).[70,71] From this value we find that the lower edge of the $4f^15d^1$ band lies at ~48 900 cm^{-1}. This is very close to the experimental value of 48 800 cm^{-1} reported in Ref. 73. Therefore, the lowest $4f^15d^1$ level at 48 900 cm^{-1} lies above the $^1S_0$ level of the $4f^2$ configuration (46 600 cm^{-1}) when the system is excited from the $^3H_4(4f^2)$ ground state.

TABLE II. Matrix elements $\langle\alpha|H_{CF}(d)|\beta\rangle$ ($\alpha,\beta=x^2-y^2$, xy, z^2, zx, and yz) of $H_{CF}(d)$ of the $5d$ electron for the ground-state geometry and for the excited-state geometry of the rare-earth site in $LaPO_4$ (in cm^{-1}). Matrix elements are obtained using Eq. (12) with the AOM parameters $e_\sigma(R_0)=7500$ cm^{-1} and $e_\pi(R_0)/e_\sigma(R_0)=0.25$ ($R_0=2.59$ Å and $n=7$); geometrical parameters (the θ_k and φ_k angles and metal-ligand distances R involved in Eq. (12) are obtained from DFT calculations (Fig. 2).

Ground-state geometry					
	x^2-y^2	xy	z^2	zx	yz
x^2-y^2	2955	1455	1744	−1590	−1923
xy	1455	−1270	−192	−265	−3255
z^2	1744	−192	4008	3307	1709
zx	−1590	−265	3307	−2452	837
yz	−1923	−3255	1709	837	−3240
Excited-state geometry					
	x^2-y^2	xy	z^2	zx	yz
x^2-y^2	2065	486	1549	−501	−2446
xy	486	−422	293	1404	−4756
z^2	1549	293	5079	3872	5115
zx	−501	1404	3872	−546	−529
yz	−2446	−4756	5115	−529	−6175

The calculated total energy extension of the $4f^15d^1$ band in $LaPO_4:Pr^{3+}$ is about 25 000 cm^{-1} (~3 eV; see Table III); this implies that the upper $4f^15d^1$ levels lie in the conduction band of $LaPO_4$ (Fig. 5). The energy density of $4f^15d^1$ states (140 energy levels within 3 eV; see the Appendix) is very high as compared to that of the $5d$ states of Ce^{3+} ion in $LaPO_4$ (five energy levels within 1.5 eV; see Table I); therefore, nonradiative relaxation processes within the $4f^15d^1$ energy band of Pr^{3+} are expected to be very fast. The CF and spin-orbit interactions cause a strong mixing of $^{2S+1}L_j$ states of the $4f^15d^1$ configuration. In fact, singlet and triplet $^{2S+1}L(4f^15d^1)$ terms of Pr^{3+} are strongly mixed in $LaPO_4$ due to a combined effect of a large $5d$ CF energy and strong $4f$ and $5d$ spin-orbit interactions; in particular, the lowest $4f^15d^1$ state (which is a singlet ^1G state in the absence of spin-orbit interaction) has a considerable (~25%) triplet component (Table III, in which only the leading triplet component ^3F is shown). Strong singlet-triplet mixing should increase considerably the intensities of spin-forbidden $4f^2\rightarrow4f^15d^1$ optical transitions.

The absolute energy positions of $4f^15d^1$ states for the excited-state geometry of the Pr site are determined similarly to the case of $LaPO_4:Ce^{3+}$. First, we calculate the absolute energy position of the centroid of the $4f^15d^1$ band for the ground-state geometry [59 141 cm^{-1}; see Fig. 5(a)], and then we calculate the relative $4f^15d^1$ centroid energy for the excited-state geometry and set it to the absolute centroid energy equal to 59 141 cm^{-1} [Fig. 5(b)]. In this way, we obtain the absolute energy levels of $4f^15d^1$ states and the Stokes shift, 3610 cm^{-1}. The latter is again determined by the dif-

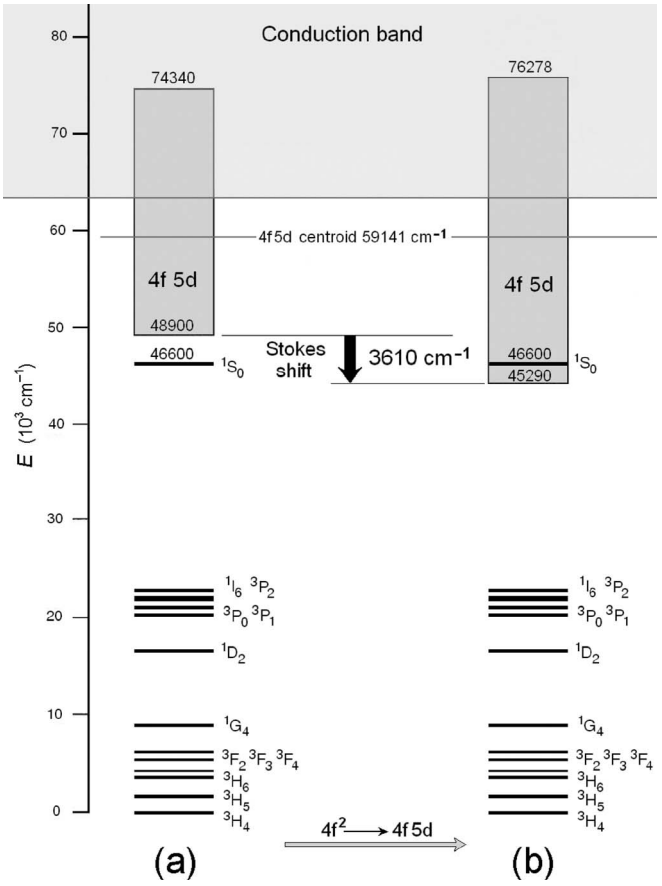

FIG. 5. The origin of the Stokes shift in $LaPO_4:Pr^{3+}$, (a) the energy level scheme of Pr^{3+} for the ground-state geometry, (b) the energy level scheme of Pr^{3+} for the excited-state geometry. The Stokes shift is measured by the difference between the energy distances from the $4f^15d^1$ centroid and the lowest $4f^15d^1$ levels for the excited-state ($4f^15d^1$) and the ground-state ($4f^2$) geometries of the Pr site.

ference of the energy distances between the centroid position and the lowest $4f^15d^1$ level for the excited-state and ground-state geometries of the Pr site; see Fig. 5.

These results show that a large Stokes shift gives rise to dramatic changes in the order of energy levels at the bottom of the $4f^15d^1$ band. In the excited-state geometry, the lower edge of the $4f^15d^1$ band shifts downward to approximately 45 000 cm^{-1}; therefore, the $^1S_0(4f^2)$ level (46 600 cm^{-1}) lies now within the $4f^15d^1$ band [Fig. 5(b)]. As a result, $4f$-$4f$ transitions from the $^1S_0$ level are not observed in the room temperature luminescence spectra of $LaPO_4:Pr^{3+}$.[73,74] This is in contrast to the luminescence behavior of Pr^{3+} in $SrSO_4$ and $BaSO_4$ matrices, in which $^1S_0 \rightarrow {}^{2S+1}L_j(4f^2)$ emitting transitions are observed.[24,75] The $5d$ energy levels of Ce^{3+} ions in $LaPO_4$ are very similar to those of Ce^{3+} ion in $SrSO_4$ and $BaSO_4$, both in the total amplitude of the CF splitting (about 12 000 cm^{-1}) and in the $5d$ centroid position. In the absorption spectra, the lowest $4f^15d^1$ state of Pr^{3+} ions lies at 50200 cm^{-1} in $SrSO_4$ and at 50 400 cm^{-1} in $BaSO_4$ (Ref. 75); this value is very close to the calculated energy in $LaPO_4:Pr^{3+}$, 48 900 cm^{-1}. The difference in the luminescence spectra originates from the Stokes shift of $5d$ levels, which is considerably smaller in $SrSO_4$ and $BaSO_4$ than in $LaPO_4$. As a consequence, the lower edge of the $4f^15d^1$ band in the sulfates is still above the $^1S_0$ state even upon the geometry relaxation of the Pr^{3+} site in the excited state. In contrast, in $CaSO_4:Pr^{3+}$ the lowest $4f^15d^1$ state lies below the $^1S_0$ state due to a much larger $5d$ CF splitting energy (~18 000 cm^{-1} in $CaSO_4$ vs ~12 000 cm^{-1} in $SrSO_4$ and $BaSO_4$).[75] It is noteworthy that the calculated $5d$ CF energy of $LaPO_4:Ce^{3+}$ in the excited-state geometry is close to that in $CaSO_4$ [Table I and Fig. 4(b)]; this is also supportive of the above conclusion.

IV. DISCUSSION AND CONCLUSIONS

In this paper, a theoretical approach for calculations of the energy level structure and the Stokes shift of excited $4f^{N-1}5d$ states of trivalent rare-earth ions is developed. It involves first-principles calculations for determining the structure of the metal sites, a model Hamiltonian for parametric calculations of $4f^{N-1}5d$ states, and angular-overlap model calculations for $5d$ electrons; some approximations are also used. The combination of these elements provides a very efficient tool for the description of $4f^{N-1}5d$ states for low-symmetry metal sites and enables to calculate the Stokes shift of the $5d$-$4f$ emission. This approach is applied to $LaPO_4:Ce^{3+}$ and $LaPO_4:Pr^{3+}$, in which the rare-earth sites have no symmetry elements. At the first step, the geometry parameters of the cerium site in $LaPO_4:Ce^{3+}$ were obtained from plane-wave DFT pseudopotential calculations for the ground and excited states of Ce^{3+}. At the next step, the obtained geometries of the Ce^{3+} site were employed in calculations of the crystal-field potential of the $5d$ electrons and the Stokes shift in terms of the angular-overlap model. AOM calculations have resulted in a good correspondence between experimental and calculated CF splitting patterns of $5d$ states of Ce^{3+} ions in $LaPO_4$. The Stokes shifts for $LaPO_4:Ce^{3+}$ estimated from the DFT calculations (4342 cm^{-1}) and from parametric model calculations (3980 cm^{-1}) are in a reasonable agreement with the experimental Stokes shift (4880 cm^{-1}). The $5d$ CF potential obtained for $LaPO_4:Ce^{3+}$ is then used to calculate the energy spectrum of $4f^15d^1$ states and the Stokes shift in $LaPO_4:Pr^{3+}$. The calculated Stokes shift of $LaPO_4:Pr^{3+}$ is also large, 3610 cm^{-1}. This leads to a crossover of the lowest $4f^15d^1$ level and the highest $^1S_0$ level of the $4f^2$ configuration upon the $4f$-$5d$ excitation on Pr^{3+} ion. In the excited-state geometry, the lower edge of the Pr^{3+} $4f^15d^1$ band lies below the $^1S_0$ level; this prevents $4f$-$4f$ optical transitions from the $^1S_0$ level in $LaPO_4:Pr^{3+}$, in which only intense $4f^15d^1 \rightarrow 4f^2$ interconfigurational optical transitions are observed in the emission spectrum at room temperature. This approach can directly be employed for other many-electron rare-earth ions in various host matrices, without limitations on the local symmetry of the metal sites. This opens up possibilities for the study of very rich and complicated optical properties of $4f^{N-1}5d$ states of rare-earth ions.

APPENDIX

See Table III for the calculated energy positions and compositions of wave functions of $4f^15d^1$ states in $LaPO_4:Pr^{3+}$.

TABLE III. Calculated energy positions (cm^{-1}) and compositions of wave functions of $4f^15d^1$ states in $LaPO_4:Pr^{3+}$. These energies refer to absorption spectra (the ground-state geometry of the rare-earth site); in the emission spectra, $4f^15d^1$ levels shift downward due to the Stokes shift.

E (cm^{-1})	Wave function $^{2S+1}L(4f^15d^1)$ composition (%)[a]				Continued				
48900	49	^{1}G	13	^{3}F	58841	24	^{3}G	21	^{3}H
49078	35	^{3}F	22	^{1}G	58930	34	^{3}H	30	^{3}G
49168	43	^{3}F	33	^{3}H	59067	34	^{3}H	18	^{1}D
49214	37	^{3}F	26	^{3}H	59282	46	^{3}H	15	^{3}F
49243	41	^{3}H	30	^{3}F	59293	45	^{3}H	15	^{3}F
49455	34	^{3}H	28	^{3}G	59639	33	^{3}H	21	^{1}F
49507	29	^{3}H	27	^{1}G	59939	58	^{3}H	14	^{3}P
49588	30	^{3}H	25	^{1}G	60159	37	^{3}H	25	^{1}F
49695	44	^{3}H	17	^{3}G	60372	37	^{1}F	22	^{1}H
50437	41	^{3}G	23	^{3}F	60851	36	^{3}G	16	^{3}F
50619	31	^{3}G	29	^{3}F	60868	28	^{3}G	23	^{3}F
50755	34	^{3}G	23	^{3}H	60975	32	^{3}G	25	^{3}F
50878	32	^{1}G	25	^{3}F	61020	24	^{3}F	21	^{3}H
50933	28	^{1}G	22	^{3}G	61066	25	^{3}G	23	^{3}F
51174	37	^{3}F	21	^{3}H	61267	28	^{3}F	20	^{3}H
51294	38	^{3}H	34	^{3}F	61452	25	^{1}F	23	^{3}G
51447	42	^{3}H	22	^{3}F	61613	30	^{3}F	26	^{3}G
51478	38	^{3}H	18	^{3}F	61719	35	^{3}G	17	^{3}F
51685	40	^{3}H	19	^{3}F	61755	34	^{3}G	25	^{3}F
51864	25	^{3}H	22	^{3}G	61846	37	^{3}G	22	^{3}F
52073	37	^{3}H	23	^{3}G	62342	28	^{3}G	18	^{3}D
52314	26	^{3}F	26	^{3}H	62523	25	^{3}H	25	^{3}D
52424	25	^{3}G	25	^{3}H	62786	24	^{3}G	23	^{3}D
52463	50	^{3}F	25	^{3}G	62896	23	^{3}H	21	^{3}D
52531	38	^{3}H	22	^{3}G	63082	30	^{3}G	21	^{3}F
52569	32	^{3}G	26	^{3}H	63122	28	^{3}G	26	^{3}D
52653	31	^{3}F	30	^{3}H	63383	23	^{3}G	22	^{3}D
52715	35	^{3}G	29	^{3}F	63619	28	^{3}F	25	^{3}H
52824	26	^{3}G	22	^{3}H	63766	30	^{3}F	29	^{3}G
52950	31	^{3}H	21	^{3}G	63788	24	^{3}G	18	^{3}D
53057	39	^{3}H	19	^{3}F	63848	29	^{3}G	20	^{3}H
53179	24	^{3}H	23	^{3}G	63902	27	^{3}D	23	^{3}H
53281	25	^{3}F	22	^{3}H	64030	26	^{3}H	25	^{3}F
53664	36	^{3}G	25	^{3}H	64173	27	^{3}G	26	^{3}H
53698	35	^{3}H	24	^{3}G	64227	21	^{3}G	18	^{3}H
53736	27	^{3}G	24	^{3}H	64419	35	^{3}D	21	^{3}G
53922	27	^{3}H	24	^{3}G	64517	27	^{3}D	21	^{3}G
53967	40	^{3}H	20	^{3}F	64597	31	^{3}D	21	^{3}H
54148	37	^{3}H	18	^{3}G	64673	36	^{3}G	28	^{3}F
54309	25	^{3}H	24	^{3}F	64732	42	^{3}G	25	^{3}F
54417	42	^{3}G	26	^{3}H	64983	19	^{3}D	19	^{3}P
54502	37	^{3}G	24	^{3}F	65041	24	^{3}P	21	^{3}H
54731	30	^{3}H	26	^{3}G	65155	34	^{3}P	22	^{3}G
54791	31	^{3}H	26	^{3}G	65298	61	^{3}P	16	^{3}H
54904	39	^{3}H	14	^{3}G	65562	29	^{3}D	21	^{3}H
54951	32	^{3}H	21	^{3}G	65635	34	^{3}D	24	^{3}H

TABLE III. (*Continued.*)

E (cm^{-1})	Wave function $^{2S+1}L(4f^15d^1)$ composition (%)[a]				Continued				
55100	26	^{3}H	17	^{3}F	65644	27	^{3}D	24	^{3}P
55322	26	^{3}H	19	^{3}G	65751	30	^{3}D	22	^{3}H
55345	34	^{3}H	20	^{3}G	65857	34	^{3}D	20	^{3}H
55363	30	^{3}G	27	^{3}H	66103	39	^{3}D	26	^{3}G
55565	32	^{3}G	29	^{3}H	66167	44	^{3}D	22	^{3}H
55835	54	^{3}H	11	^{3}D	66463	36	^{1}H	23	^{3}P
55893	44	^{3}H	14	^{3}G	66793	27	^{1}H	27	^{3}P
55925	34	^{3}H	21	^{3}G	66905	40	^{1}H	15	^{3}P
56016	22	^{3}H	20	^{1}D	67248	52	^{3}P	22	^{3}H
56098	40	^{3}H	16	^{3}G	67320	53	^{3}P	21	^{3}H
56158	49	^{3}H	17	^{3}G	67346	58	^{3}P	23	^{3}H
56325	23	^{3}H	19	^{3}G	67557	50	^{3}P	22	^{3}H
56388	28	^{3}G	19	^{3}H	67567	58	^{3}P	26	^{3}H
56520	24	^{3}H	18	^{1}D	68118	59	^{1}H	12	^{1}F
57052	28	^{3}H	19	^{3}G	68698	42	^{1}H	32	^{1}F
57275	21	^{3}H	19	^{3}G	68885	58	^{1}H	17	^{1}F
57438	39	^{3}H	15	^{3}D	69354	64	^{1}H	15	^{1}F
57850	23	^{3}H	15	^{3}G	69823	60	^{1}H	25	^{1}F
57884	20	^{3}G	19	^{1}G	69945	72	^{1}H	11	^{1}F
58073	25	^{3}H	19	^{3}G	70908	79	^{1}H	13	^{1}F
58230	24	^{3}H	22	^{3}G	70980	79	^{1}H	13	^{1}F
58334	33	^{3}G	23	^{3}F	73693	58	^{1}P	31	^{1}H
58408	29	^{3}G	23	^{3}F	74011	58	^{1}P	33	^{1}H
58699	34	^{3}G	29	^{3}H	74340	58	^{1}P	34	^{1}H

[a]Only two leading ^{2S+1}L terms of the $4f^15d^1$ configuration are indicated in the composition of the wave functions.

[1] B. Blasse and B. Grabmaier, *Luminescent Materials* (Springer, Berlin, 1994), p. 130.

[2] R. T. Wegh, H. Donker, K. D. Oskam, and A. Meijerink, Science **283**, 663 (1999).

[3] M. F. Reid, L. van Pieterson, R. T. Wegh, and A. Meijerink, Phys. Rev. B **62**, 14744 (2000).

[4] L. X. Ning, C. K. Duan, S. D. Xia, M. F. Reid, and P. A. Tanner, J. Alloys Compd. **366**, 34 (2004).

[5] P. S. Peijzel, P. Vergeer, A. Meijerink, M. F. Reid, L. A. Boatner, and G. W. Burdick, Phys. Rev. B **71**, 045116 (2005).

[6] L. van Pieterson, M. F. Reid, R. T. Wegh, S. Soverna, and A. Meijerink, Phys. Rev. B **65**, 045113 (2002).

[7] L. van Pieterson, M. F. Reid, G. W. Burdick, and A. Meijerink, Phys. Rev. B **65**, 045114 (2002).

[8] M. F. Reid, L. van Pieterson, and A. Meijerink, J. Alloys Compd. **344**, 240 (2002).

[9] J. Andriessen, O. T. Antonyak, P. Dorenbos, P. A. Rodnyi, G. V. Stryganyuk, C. W. E. van Eijk, and A. S. Voloshinovskii, Opt. Commun. **178**, 355 (2000).

[10] M. Marsman, J. Andriessen, and C. W. E. van Eijk, J. Lumin. **87-89**, 1023 (2000).

[11] M. Marsman, J. Andriessen, and C. W. E. van Eijk, Phys. Rev. B **61**, 16477 (2000).

[12] J. Andriessen, M. Marsman, and C. W. E. van Eijk, J. Phys.: Condens. Matter **13**, 5611 (2001).

[13] P. Dorenbos, J. Lumin. **91**, 91 (2000).

[14] W. W. Piper, J. A. DeLuca, and F. S. Ham, J. Lumin. **8**, 344 (1974).

[15] J. L. Sommerdijk, A. Bril, and A. W. de Jager, J. Lumin. **8**, 341 (1974).

[16] J. L. Sommerdijk, A. Bril, and A. W. de Jager, J. Lumin. **9**, 288 (1974).

[17] A. P. Vink, P. Dorenbos, J. T. M. de Haas, H. Donker, P. A. Rodnyi, A. G. Avanesov, and C. W. E. van Eijk, J. Phys.: Condens. Matter **14**, 8889 (2002).

[18] S. Kück and I. Sokólska, J. Electrochem. Soc. **149**, J27 (2002).

[19] S. Kück, I. Sokólska, M. Henke, T. Scheffler, and E. Osiac, Phys. Rev. B **71**, 165112 (2005).

[20] A. M. Srivastava and W. W. Beers, J. Lumin. **71**, 285 (1997).

[21] A. M. Srivastava, D. A. Doughty, and W. W. Beers, J. Electrochem. Soc. **143**, 4113 (1996).

[22] A. M. Srivastava, D. A. Doughty, and W. W. Beers, J. Electrochem. Soc. **144**, L190 (1997).

[23] A. P. Vink, P. Dorenbos, and C. W. E. van Eijk, Phys. Rev. B **66**, 075118 (2002).

[24] E. van der Kolk, P. Dorenbos, A. P. Vink, R. C. Perego, C. W. E.

van Eijk, and A. R. Lakshmanan, Phys. Rev. B **64**, 195129 (2001).
[25] S. Baroni, A. Dal Corso, S. de Gironcoli, P. Giannozzi, C. Cavazzoni, G. Ballabio, S. Scandolo, G. Chiarotti, P. Focher, A. Pasquarello, K. Laasonen, A. Trave, R. Car, N. Marzari, and A. Kokalj, http://www.pwscf.org/
[26] D. Vanderbilt, Phys. Rev. B **41**, 7892 (1990).
[27] M. Mikami and S. Nakamura, J. Alloys Compd. **408-412**, 687 (2006).
[28] H. J. Monkhorst and J. D. Pack, Phys. Rev. B **13**, 5188 (1976).
[29] J. P. Perdew, J. A. Chevary, S. H. Vosko, K. A. Jackson, M. R. Pederson, D. J. Singh, and C. Fiolhais, Phys. Rev. B **46**, 6671 (1992).
[30] Y. Ni, J. M. Hughes, and A. N. Mariano, Am. Mineral. **80**, 21 (1995).
[31] A. T. Aldred, Acta Crystallogr., Sect. B: Struct. Sci. **40**, 569 (1984).
[32] D. F. Mullica, D. A. Grossie, and L. A. Boatner, J. Solid State Chem. **58**, 71 (1985).
[33] K. C. Mishra, I. Osterloh, H. Anton, B. Hannebauer, P. C. Schmidt, and K. H. Johnson, J. Mater. Res. **12**, 2183 (1997).
[34] K. C. Mishra, I. Osterloh, H. Anton, B. Hannebauer, P. C. Schmidt, and K. H. Johnson, J. Lumin. **72-74**, 144 (1997).
[35] E. Nakazawa and F. Shiga, J. Lumin. **15**, 255 (1977).
[36] M. S. Hybertsen and S. G. Louie, Phys. Rev. Lett. **55**, 1418 (1985).
[37] F. Aryasetiawan and O. Gunnarsson, Rep. Prog. Phys. **61**, 237 (1998).
[38] W. T. Carnall, G. L. Goodman, K. Rajnak, and R. S. Rana, J. Chem. Phys. **90**, 3443 (1989).
[39] C. Görller-Walrand and K. Binnemans, in *Handbook on the Physics and Chemistry of Rare Earths*, edited by K. A. Gschneidner, Jr. and L. Eyring (North-Holland, Amsterdam, 1996), Vol. 23, p. 121.
[40] D. J. Newman and B. K. C. Ng, *Crystal Field Handbook* (Cambridge University Press, Cambridge, 2000).
[41] B. G. Wybourne, *Spectroscopic Properties of the Rare Earths* (Interscience, New York, 1965).
[42] C. A. Morrison and R. P. Leavitt, in *Handbook on the Physics and Chemistry of Rare Earths*, edited by K. A. Gschneidner, Jr. and L. Eyring (North-Holland, Amsterdam, 1982), Vol. 5, Chap. 46.
[43] E. Antic-Fidancev, J. Holsa, M. Lemaitre-Blaise, and P. Porcher, J. Phys.: Condens. Matter **3**, 6829 (1991).
[44] C. Rudowicz and J. Qin, J. Lumin. **110**, 39 (2004).
[45] C. Rudowicz and S. K. Misra, Appl. Spectrosc. Rev. **36**, 11 (2001).
[46] G. W. Burdick and M. F. Reid, Mol. Phys. **102**, 1141 (2004).
[47] L. van Pieterson, R. T. Wegh, A. Meijerink, and M. F. Reid, J. Chem. Phys. **115**, 9382 (2001).
[48] T. Chen, C. K. Duan, S. D. Xia, and M. Yin, J. Lumin. **122–123**, 51 (2007).
[49] P. A. Tanner, C. S. K. Mak, M. D. Faucher, W. M. Kwok, D. L. Phillips, and V. Mikhailik, Phys. Rev. B **67**, 115102 (2003).
[50] C. K. Jorgensen, R. Pappalardo, and H. H. Schmidtke, J. Chem. Phys. **39**, 1422 (1963).
[51] C. E. Schaffer, Struct. Bonding (Berlin) **5**, 68 (1968).
[52] C. E. Schaffer and C. K. Jorgensen, Mol. Phys. **9**, 401 (1965).
[53] M. Kilber, Aust. J. Chem. **35**, 231 (1982).
[54] M. Gerloch, J. H. Harding, and G. Wooley, Struct. Bonding (Berlin) **46**, 1 (1981).
[55] L. Banci, A. Bencini, C. Benelli, D. Gatteschi, and C. Zanchini, Struct. Bonding (Berlin) **52**, 37 (1982).
[56] M. Gerloch and R. F. Mc Meeking, J. Chem. Soc. Dalton Trans. **1981**, 1714.
[57] A. Bencini, C. Benelli, and D. Gatteschi, Coord. Chem. Rev. **60**, 131 (1984).
[58] M. Moreno, M. T. Barriuso, J. A. Aramburu, P. Garcıa-Fernandez, and J. M. Garcıa-Lastra, J. Phys.: Condens. Matter **18**, R315 (2006).
[59] P. V. Bernhardt and P. Comba, Inorg. Chem. **32**, 2798 (1993).
[60] C. E. Schaffer, Proc. R. Soc. London, Ser. A **297**, 96 (1967).
[61] C. E. Schaffer, Struct. Bonding (Berlin) **14**, 69 (1973).
[62] D. Gatteschi and L. Sorace, J. Solid State Chem. **159**, 253 (2001).
[63] D. Hernández, F. Rodríguez, M. Moreno, and H. U. Güdel, Physica B (Amsterdam) **265**, 186 (1999).
[64] M. Moreno, M. T. Barriuso, and J. A. Aramburu, J. Phys.: Condens. Matter **4**, 9481 (1992).
[65] M. Grinberg, Opt. Mater. (Amsterdam, Neth.) **28**, 26 (2005).
[66] J. Barzowska, M. Grinberg, and T. Tsuboi, Radiat. Eff. Defects Solids **158**, 39 (2003).
[67] S. Watanabe, T. Ishii, K. Fujimura, and K. Ogasawara, J. Solid State Chem. **179**, 2438 (2006).
[68] M. G. Brik and K. Ogasawara, Spectrosc. Lett. **40**, 221 (2007).
[69] M. G. Brik, J. Alloys Compd. **454**, 38 (2008).
[70] M. V. Hoffman, J. Electrochem. Soc. **118**, 1508 (1971).
[71] A. Mayolet, Ph.D. thesis, Universite de Paris XI Orsay, 1995.
[72] R. D. Cowan, *The Theory of Atomic Structure and Spectra* (University of California, Berkeley, 1981).
[73] E. Nakazawa and F. Shiga, Jpn. J. Appl. Phys., Part 1 **42**, 1642 (2003).
[74] W. W. Beers, H. A. Comanzo, and A. M. Srivastava, in *Physics and Chemistry of Luminescent Materials*, Proceedings of the Eight International Symposium Vols. 99–40, edited by C. Ronda, L. Shea, and A. M. Srivastava (Electrochemical Society, New York, 2000), p. 168.
[75] A. P. Vink, E. van der Kolk, P. Dorenbos, and C. W. E. van Eijk, J. Alloys Compd. **341**, 338 (2002).